Interaction of anatomic and quantum noise in DBT power spectrum

Amar Kavuri, Nathaniel R. Fredette, Mini Das

Amar Kavuri, Nathaniel R. Fredette, Mini Das, "Interaction of anatomic and quantum noise in DBT power spectrum," Proc. SPIE 10577, Medical Imaging 2018: Image Perception, Observer Performance, and Technology Assessment, 105770G (7 March 2018); doi: 10.1117/12.2295218

SPIE.

Event: SPIE Medical Imaging, 2018, Houston, Texas, United States

Interaction of anatomic and quantum noise in DBT Power Spectrum

Amar Kavuri [a], Nathaniel R. Fredette [a] and Mini Das [a,b,*]

[a]Department of Biomedical Engineering, University of Houston, Houston, TX, USA
[b]Department of Physics, University of Houston, Houston, TX, USA
*Email: mdas@uh.edu

ABSTRACT

In x-ray breast images, anatomical variations have been characterized by slope of the noise power spectrum (NPS) that follows an inverse power-law relationship. Prior literature has reported that this slope (β) changes with imaging modality (DBT vs. mammography) and with different reconstruction algorithms and filters for the same breast structures. In this paper, we assessed the relative contributions of anatomic and quantum noise in the estimated magnitude of β. This is achieved via simulations with varying levels of quantum noise and examining contributions of noise filters. The calculations were performed on simulated DBT images from anthropomorphic software breast phantoms under varying acquisition and reconstruction/filter parameters. Our results indicate that variations in β cannot be solely considered as an indicator of reduced "anatomic noise" and hence potentially improved detectability in those images; presence of quantum noise and view aliasing artifacts in anatomical region always lowered the value of β.

Keywords: beta, noise power spectrum, power law, anatomic noise, quantum noise, DBT, denoising, Adaptive Wiener filter

1. INTRODUCTION

Digital breast tomosynthesis (DBT), contrary to Digital mammography (DM), generates 3D images that afford improvements in the perceptibility of anatomical features and, therefore, can facilitate the detection of cancer and other malignancies.[1,2] Major challenge in DM relates to tissue superimposition, which can obscure or mimic abnormalities. By contrast, the 3D slices of DBT show a notable reduction in tissue superimposition. In the literature, this superimposed tissue structure is referred to as anatomic noise and it is characterized using the noise power spectrum(NPS). Bochud et al.[3] and Burgess[4] showed that this NPS follows a power law and can be expressed by relation:

$$NPS_a(f) = Kf^{-\beta} \tag{1}$$

where NPS_a is the noise power spectrum where anatomical variation dominates, f is the spatial frequency components in image and K describes the magnitude of fluctuation, and β denotes the degree of correlation of the variations. The estimated value for β is used to define the anatomical variability.

Engstrom et al.[5] estimated power law coefficient (β) of tomosynthesis projections and reconstructions of 55 patient breasts and found that β for the tomosynthesis projections had a mean of 3.06, while for the reconstructions the value of β was 2.87, with the difference being statistically significant. Chen et al.[6] found that the mean values of β of 23 patients in DBT, and mammography images were 3.06–3.10, and 3.17–3.30. Vancamberg et al.[7], Hu et.al.[8], however, have shown that β varies with different reconstruction methods and reconstruction filters in DBT even though original structure is same. However, relative contributions of anatomic and quantum noise in estimating the magnitude of β is not well understood.

In DBT, a set of x-ray projections is acquired with a total dose same as Mammography. Increase in quantum noise due to the low dose in each DBT projection would pose challenges in detecting small scale signals[9]. Cockmartian et al.[10] have shown that change in imaging dose affects DBT projections and reconstructed images differently, this is often due to the use of apodization filter. Effects of denoising filters were investigated by Oliveira et al.[11] and Borges et al.[12]. In this paper, a systematic investigation is conducted to understand the interplay of anatomic and quantum noise in the estimated power law exponent β.

Medical Imaging 2018: Image Perception, Observer Performance, and Technology Assessment, edited by Robert M. Nishikawa, Frank W. Samuelson, Proc. of SPIE Vol. 10577, 105770G
 · doi: 10.1117/12.2295218

2. MATERIALS AND METHODS

2.1. Image generation and reconstruction:

The digital breast phantoms used in this study are three-dimensional anthropomorphic breast models generated by Bakic et al.[13] at the University of Pennsylvania. Phantoms were categorized based on densities with volumetric glandular fractions (VGFs) of approximately 25% and 50%. The lesion targets were homogeneous spheres with an 8-mm diameter. The abnormal cases were simulated by substituting the lesion to the phantom at a random depth in the glandular region prior to the projection imaging. Noise and blur were added based on a serial cascade model. However, scatter blur was not accounted for. We used an angular span of 60° with projection number P∈{3, 7, 11, 15, 19, 21, 25, 31, 35, 41, 45, 51}. These projected images were reconstructed to a three-dimensional image of 760×191×240 voxels, each having an in-plane size of 0.27mm × 0.27mm. Subsequently, a three-dimensional Butterworth filter with a cutoff of frequency 0.25 cycles/pixel (0.926 mm^{-1}) was implemented. Coronal images of one-millimeter thickness were produced by applying a boxcar averaging of five slices. Axial slices were not considered in this study as they follow a double wedge spectral density[14]. These coronal images were used for the human observer studies in our earlier work[15]. In this study, we used images generated with three different systems: (1) noisy system, (2) noiseless system where electronic noise and quantum noise were absent, and (3) denoising system where noisy projections were filtered and its description is as follows.

2.2. Denoising:

We let f represent the noiseless projection image and a simple model is used to describe noise-degradation process in DBT projections as,

$$g(x,y) = f(x,y) + n(x,y) \tag{2}$$

Where $g(x,y)$ is the noisy DBT projection with additive white noise $n(x,y)$ at all coordinates x and y. DBT projections are filtered using wiener and is defined as[16],

$$\hat{f}(x,y) = \bar{f}(x,y) + \frac{{\sigma_f}^2(x,y)}{{\sigma_f}^2(x,y) + {\sigma_n}^2(x,y)}[g(x,y) - \bar{g}(x,y)] \tag{3}$$

Where $\hat{f}(x,y)$ is the estimate of noiseless image, $\bar{f}(x,y)$ and ${\sigma_f}^2(x,y)$ are the mean and variance of the noiseless image; $\bar{g}(x,y)$ is the mean of the noisy image $g(x,y)$; and ${\sigma_n}^2(x,y)$ represent the variance of noise. As the input image $f(x,y)$ is not known, accurate estimate of the parameters $\bar{f}(x,y)$ and ${\sigma_f}^2(x,y)$ is not possible. In addition, Wiener filter works well for noisy projection $g(x,y)$ corrupted by Gaussian additive noise.[16] Vieira et.al[17] have shown that performance of Wiener filter is improved with the use of Anscombe transform. Moreover, the transformed variable is approximately Gaussian random variable with noise variance of unity and zero mean.[17] The Anscombe transform of the noisy image is given by[18],

$$t(x,y) = 2\sqrt{g(x,y) + \frac{3}{8}} \tag{4}$$

Where $t(x,y)$ represents the transformed image with additive noise with unit variance. After the Anscombe transform, Wiener filter can be rewritten as[17],

$$\hat{s}(x,y) = \bar{t}(x,y) + \frac{{\sigma_t}^2(x,y)}{{\sigma_t}^2(x,y) + 1}[t(x,y) - \bar{t}(x,y)] \tag{5}$$

Where $\bar{t}(x,y)$ and ${\sigma_t}^2(x,y)$ are the mean and variance of the transformed noisy image. These parameters are estimated for each pixel location using an adaptive kernel. The kernel sizes were chosen based on the signal activity of the area (for low signal activity - 7×7, for moderate activity - 5×5, and for areas with sharp transitions - 2×5). The inverse Anscombe must be applied on filtered image $\hat{s}(x,y)$ to estimate the noise free projection image. The inverse Anscombe transformation is described as[19],

$$\hat{f}(x,y) = \frac{1}{4}\hat{s}^2(x,y) + \frac{1}{4\hat{s}(x,y)}\sqrt{\frac{3}{2}} - \frac{11}{8\hat{s}^2(x,y)} + \frac{5}{8\hat{s}^3(x,y)}\sqrt{\frac{3}{2}} - \frac{1}{8} \tag{6}$$

Where, $\hat{f}(x,y)$ is the estimate of the noise free input image. Fig. 1 shows an example reconstructed slice of 25% phantom with 8 mm spherical lesion on the left and corresponding denoised reconstructed slice on the right side. The black arrow indicates the location of the inserted lesion. In this paper, we investigated effect of denoising of DBT projections with Wiener filter on NPS of DBT slices.

2.3. Estimation of beta (β):

The first step in calculating β is to apply a histogram-based segmentation method to separate the breast tissue region from the background of reconstructed test image. Around 25 regions of interest (ROI) of size 90×90 (2.43cm × 2.43cm) are chosen to cover entire breast region with 50% overlap as shown in Fig. 2. ROI size is chosen empirically while ensuring that it was large enough to allow for an accurate estimate of β but not too large as to emphasize non-uniformity in the image as mentioned in Ref. [5]. Next step of calculating β is subtracting mean of the ROI from the selected ROI and then applying Hann window. Fourier transform of each ROI is computed and the low frequency components are shifted to the center. The power spectrum of each ROI is then computed as the squared modulus of Fourier transform. The average of all power spectra from the ROIs of each test image is computed then radially averaged. [0.15, 0.7] cycles/mm is maintained as linear portion of log-log plot of power spectrum as mentioned in Ref. [20], and the slope of this linear portion is computed as β.

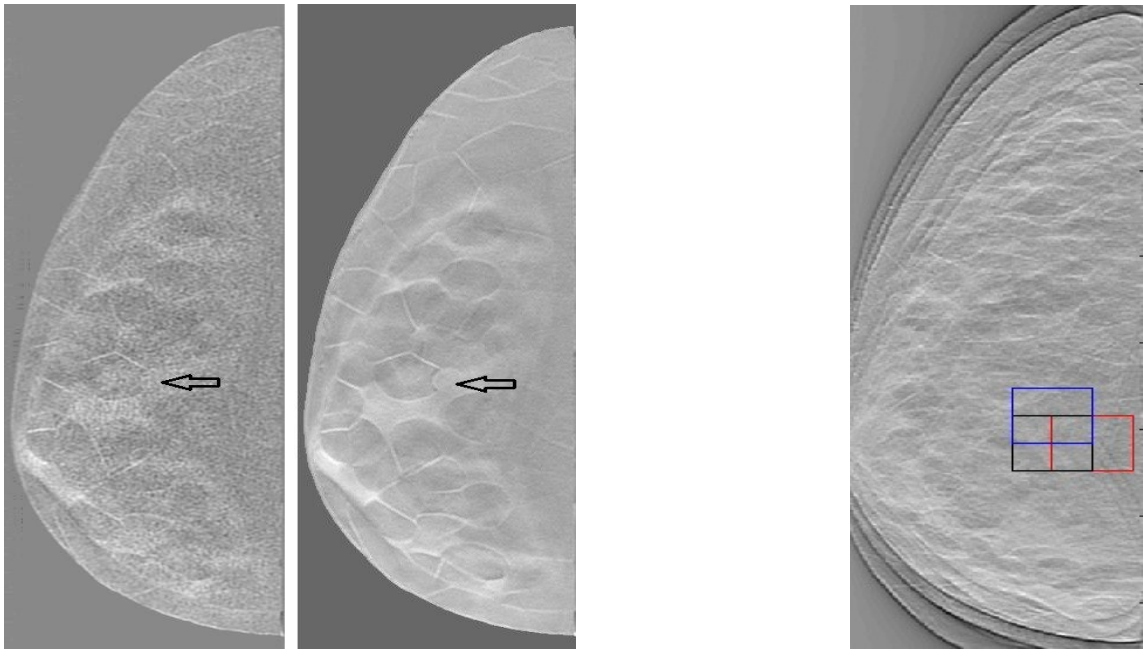

Figure 1: (left and center) Example DBT reconstructed slices generated (a) with regular noisy system and (b) with denoising system. The black arrows indicate the location of a spherical lesion and Figure 2:(right) Selection of sample regions with 50% overlap in both spatial directions to estimate noise power spectrum.

3. RESULTS

A noiseless mammography was acquired with 1.5 mGy dose and its power spectrum is plotted along with the power spectrum of a DBT center projection in Fig. 4(a). The DBT projection was acquired with 1/25th of the mammography dose. The deviation in spectra in projections due to quantum noise starts at frequency as low as 0.3 mm^{-1}, accordance with earlier observations of Engstrom et al.[5] and Cockmartian et al.[10], which is in the power law region. The lower value of β (2.68) in DBT projection is due to the presence of quantum noise in anatomical region but not due to decrease in the anatomical variability (as same structure is projected). The noisy projection was filtered using adaptive Wiener filter as described in section "Denoising". The Noise power spectrum of Wiener filtered projection was also plotted, and Fig. 4(a) shows that Wiener filter reduced quantum noise effectively at frequencies higher than 1 mm^{-1} and less effectively between 0.5 to 1 mm^{-1}. We show sample region images in Fig.3 obtained from the DM and center DBT projections. Image on the left (a) shows the DM image; image (b) is the noisy DBT center projection and (c) is Wiener filtered projection.

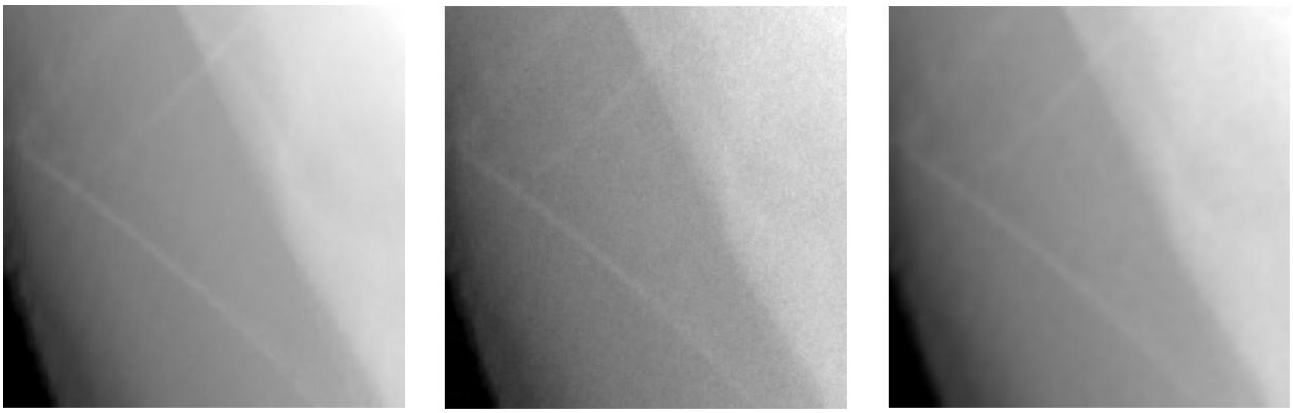

Figure 3: Image on the left (a) shows a region of noiseless mammogram; image (b) is the corresponding noisy DBT center projection and (c) is Wiener filtered center projection

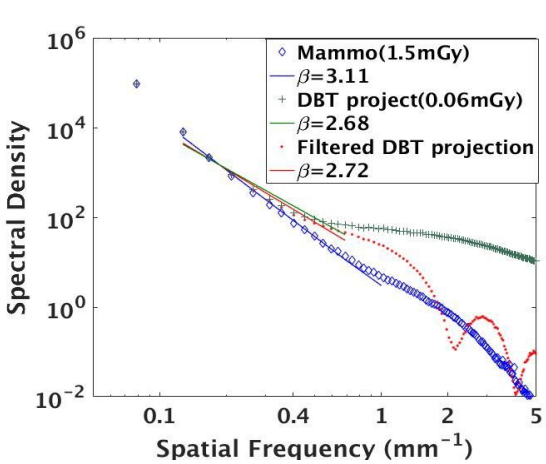

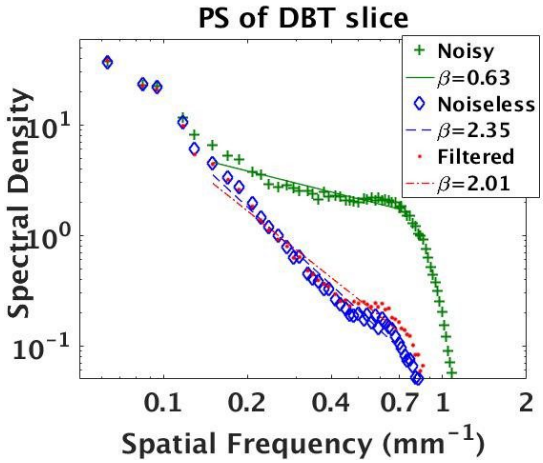

Figure 4: (a) Power spectra of a noiseless mammogram and DBT projections with and without filtering. Difference between these spectra is due to increase in quantum noise and the deviation starts at frequency as low as 0.3 mm^{-1}. (b) Power spectra of same depth reconstructed slice of noisy system, noiseless system and filtered noisy system. Influence of noise starts at frequency as low as 0.15 mm^{-1}. Filtering on projections significantly reduced effect of quantum noise on the DBT slice.

1-mm coronal slices were reconstructed from 25 equally spaced such DBT projections acquired over a 60° arc span. Power spectrum of a middle slice was plotted in Fig. 4(b), and is labeled as 'Noisy'. β of this slice was estimated as 0.63. 1-mm slices were generated with the similar strategy using noiseless system as well. The power spectrum of same depth slice was also plotted ('Noiseless') and β was estimated as 2.35. As observed in Fig.4(b), quantum noise starts to influence β at frequency as low as 0.15 mm^{-1} in reconstructed slices. The 25 noisy projections were Wiener filtered, and the 1-mm slices were reconstructed. Power spectrum of same depth slice was also plotted to understand the effect of denoising on the reconstructed slices, and it is evident in Fig.4(b) that system noise was effectively removed in the anatomical region.

β of 8 randomly selected depth axial slices for each phantom was calculated. Images were reconstructed from varying projection number from 3 to 51 from the three systems and average β of lesion free images were plotted in Fig. 5 against varying projections acquired over a 60° arc span. The length of the error bars represents twice the standard deviation of distribution of β for 48 slices. β of images generated in a regular system is plotted as 'Noisy' and noiseless system images as 'Noiseless'. The difference between average β of noisy and noiseless curves is increasing as projection number increases, this relates to the increase in the effect of system noise as the number of projections increase. The curve of filtered images shows that system noise was reduced effectively. The increase in the difference between noiseless and filtered curves as projection number increases suggests that residual noise is increasing.

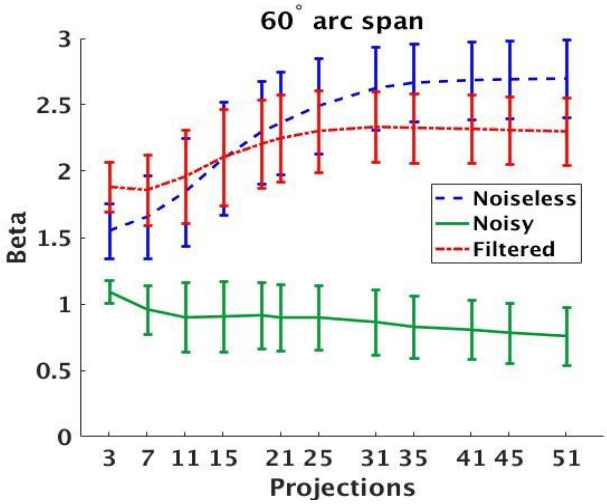

Figure 5: Average β of DBT slices of noiseless system, noisy system, and system with Wiener filter. Error bars indicate the standard deviation of distribution of β values of 48 slices.

The noiseless plot in Fig.5 shows that due to insufficient sampling at lower projection numbers, view aliasing artifacts contributed to higher frequency components of power spectrum, and results in lower value of β. As the number of projections increases these artifacts were resolved, resulting in an increase in β. The average β of noisy images in Fig.5 shows that even though increasing the number of projections reduced view aliasing artifacts, increase in the system noise negated the increase in average β.

Changes in image processing technique and system geometry appears to change β. These trends point to the fact that β cannot be a reliable factor in gauging system performance. Our preliminary investigations suggest that these trends do not correlate with human observer performance. More systematic investigations are underway to test these against human observer performance in LROC studies.

4. CONCLUSIONS

In this work, we investigated the effect of quantum noise on β of DBT projections and reconstruction slices. Results show that quantum noise starts to influence power spectrum at frequencies as low as 0.3 mm^{-1} on DBT projections and 0.15 mm^{-1} on DBT reconstruction slices. We take a closer look at the true origin of β for tomographic X-ray imaging. Our results show that the origin of β is not always simply anatomic variations but also include effects of reconstruction artifacts, quantum noise and filters. Our results suggest both quantum noise and reconstruction artifacts lower value of β. Hence, β cannot be solely considered as an indicator of reduced "anatomic noise" and hence potentially improved detectability in tomographic images. Further investigations are underway to quantitate these noise power spectral parameters and examine their potential correlation with human observer performance.

ACKNOWLEDGEMENTS

This work was partially supported by funding from the US Department of Defense (DOD) Congressionally Directed Medical Research Program (CDMRP) Breakthrough Award BC151607 and the National Science Foundation CAREER Award 1652892. We would also like to thank Dr. Predrag Bakic from the University of Pennsylvania for supplying the phantoms utilized in this study.

REFERENCES:

[1] Whelehan, P., Heywang-Kцbrunner, S.H., Vinnicombe, S.J., Hacker, A., Jaensch, A., Hapca, A., Gray, R., Jenkin, M., Lowry, K., Oeppen, R. and Reilly, M., "Clinical performance of Siemens digital breast tomosynthesis versus standard supplementary mammography for the assessment of screen-detected soft-tissue abnormalities: a multi-reader study," Clinical radiology, 72(1), pp.95-e9 (2017).

[2] Gilbert, F.J., Tucker, L. and Young, K.C., "Digital breast tomosynthesis (DBT): a review of the evidence for use as a screening tool," Clinical radiology, 71(2), pp.141-150 (2016).

[3] Bochud, F.O., Valley, J.F., Verdun, F.R., Hessler, C. and Schnyder, P., "Estimation of the noisy component of anatomical backgrounds," Medical physics, 26(7), pp.1365-1370 (1999).

[4] Burgess, A. E., "Mammographic structure: Data preparation and spatial statistics analysis," In Medical Imaging: Image Processing, vol. 3661, pp. 642-654. International Society for Optics and Photonics, (1999).

[5] Engstrom, E., Reiser, I. and Nishikawa, R.,"Comparison of power spectra for tomosynthesis projections and reconstructed images," Medical physics, 36(5), pp.1753-1758 (2009).

[6] Chen, L., Abbey, C.K., Nosratieh, A., Lindfors, K.K. and Boone, J.M., "Anatomical complexity in breast parenchyma and its implications for optimal breast imaging strategies," Medical physics, 39(3), pp.1435-1441 (2012).

[7] Vancamberg, L., Carton, A.K., Abderrahmane, I.H., Palma, G., de Carvalho, P.M., Iordache, R. and Muller, S., "Influence of DBT reconstruction algorithm on power law spectrum coefficient." In Medical Imaging: Physics of Medical Imaging, vol. 9412, p. 941236. International Society for Optics and Photonics (2015).

[8] Hu, Y.H., Masiar, M. and Zhao, W., "Breast structural noise in digital breast tomosynthesis and its dependence on reconstruction methods," In International Workshop on Digital Mammography (pp. 598-605). Springer, Berlin, Heidelberg (2010).

[9] Reiser, I. and Nishikawa, R.M., "Task-based assessment of breast tomosynthesis: Effect of acquisition parameters and quantum noise," Medical physics, 37(4), pp.1591-1600 (2010).

[10] Cockmartin, L., Bosmans, H. and Marshall, N.W., "Comparative power law analysis of structured breast phantom and patient images in digital mammography and breast tomosynthesis," Medical physics, 40(8) (2013).

[11] de Oliveira, H.C.R., Borges, L.R., Nunes, P.F., Bakic, P.R., Maidment, A.D. and Vieira, M.A., "Use of wavelet multiresolution analysis to reduce radiation dose in digital mammography," In Computer-Based Medical Systems (CBMS), IEEE 28th International Symposium on (pp. 33-37). IEEE (2015).

[12] Borges, L.R., Bakic, P.R., Foi, A., Maidment, A.D. and Vieira, M.A., "Pipeline for effective denoising of digital mammography and digital breast tomosynthesis." In Medical Imaging: Physics of Medical Imaging, vol. 10132, p. 1013206. International Society for Optics and Photonics (2017).
[13] Bakic, P.R., Albert, M., Brzakovic, D. and Maidment, A.D., "Mammogram synthesis using a 3D simulation. I. Breast tissue model and image acquisition simulation," Medical Physics, 29(9), pp.2131-2139 (2002).
[14] Gang, G.J., Tward, D.J., Lee, J. and Siewerdsen, J.H., "Anatomical background and generalized detectability in tomosynthesis and cone-beam CT," Medical physics, 37(5), pp.1948-1965 (2010).
[15] Das, M., Liang, Z. and Gifford, H.C., 2015, "Examining wide-arc digital breast tomosynthesis: optimization using a visual-search model observer." In Medical Imaging: Physics of Medical Imaging, vol. 9412, p. 94121S. International Society for Optics and Photonics (2015).
[16] Lee, J.S., "Digital image enhancement and noise filtering by use of local statistics," IEEE transactions on pattern analysis and machine intelligence, (2), pp.165-168 (1980).
[17] Vieira, M.A., Bakic, P.R. and Maidment, A.D., "Effect of denoising on the quality of reconstructed images in digital breast tomosynthesis." In Medical Imaging: Physics of Medical Imaging, vol. 8668, p. 86680C. International Society for Optics and Photonics (2013).
[18] Anscombe, F.J., "The transformation of Poisson, binomial and negative-binomial data," Biometrika, 35(3/4), pp.246-254 (1948).
[19] Makitalo, M. and Foi, A., "A closed-form approximation of the exact unbiased inverse of the Anscombe variance-stabilizing transformation" IEEE transactions on image processing, 20(9), pp.2697-2698 (2011).
[20] Lau, B.A., Reiser, I. and Nishikawa, R.M., "Issues in characterizing anatomic structure in digital breast tomosynthesis," In Medical Imaging: Physics of Medical Imaging, vol. 7961, p. 796113. International Society for Optics and Photonics (2011).